International Journal of Minerals, Metallurgy and Materials
Volume 22, Number 4, April 2015, Page 437
DOI: 10.1007/s12613-015-1091-1

Preparation of a novel PAN/cellulose acetate–Ag based activated carbon nanofiber and its adsorption performance for low-concentration SO_2

Yan-bo Wu, Jun Bi, Ting Lou, Tie-ben Song, and Hong-quan Yu

School of Environmental and Chemical Engineering, Dalian Jiaotong University, Dalian 116028, China

(Received: 26 June 2014; revised: 30 July 2014; accepted: 3 September 2014)

Abstract: Polyacrylonitrile (PAN), PAN/cellulose acetate (CA), and PAN/CA–Ag based activated carbon nanofiber (ACNF) were prepared using electrostatic spinning and further heat treatment. Thermogravimetry–differential scanning calorimetry (TG–DSC) analysis indicated that the addition of CA or Ag did not have a significant impact on the thermal decomposition of PAN materials but the yields of fibers could be improved. Scanning electron microscopy (SEM) analysis showed that the micromorphologies of produced fibers were greatly influenced by the viscosity and conductivity of precursor solutions. Fourier transform infrared spectroscopy (FT-IR) analysis proved that a cyclized or trapezoidal structure could form and the carbon scaffold composed of C=C bonds appeared in the PAN-based ACNFs. The characteristic diffraction peaks in X-ray diffraction (XRD) spectra were the evidence of a turbostratic structure and silver existed in the PAN/CA–Ag based ACNF. Brunner–Emmett–Teller (BET) analysis showed that the doping of CA and Ag increased surface area and micropore volume of fibers; particularly, PAN/CA–Ag based ACNF exhibited the best porosity feature. Furthermore, SO_2 adsorption experiments indicated that all the three fibers had good adsorption effects on lower concentrations of SO_2 at room temperature; especially, the PAN/CA–Ag based ACNF showed the best adsorption performance, and it may be one of the most promising adsorbents used in the fields of chemical industry and environment protection.

Keywords: activated carbon; nanofibers; polyacrylonitrile; electrospinning; adsorption; sulfur dioxide

1. Introduction

Activated carbon fiber (ACF) is a novel high-performance carbonaceous adsorbent material, which has found numerous applications in chemical industry and environmental engineering. Given the fact that economic development has severely worsened global pollution problems, the most effective approach to control major domestic atmospheric pollutants like SO_2, NO_x, and volatile organic compounds (VOCs) is adsorption, in which ACFs have been playing pivotal roles. Specifically, ACF materials have exhibited remarkable adsorption properties, due to their large specific surface area and even pore size distribution [1–6]. Commercially available ACF materials, which have been either impregnated with metals/metal oxides [7–10], or functionalized with suitable reagents on the surface [11], appear to be more efficient catalysts for the oxidation of SO_2, NO, and VOCs. Recently, a nanostructured activated carbon nanofiber (ACNF) has been reported, providing an effective tool for toxic substance elimination and cell/capacitor production, due to its light weight, large specific surface area, and microporosity [12–13]. Surprisingly, this novel material has exhibited superior efficiency on contaminant adsorption compared with regular ACF or metal-impregnated ACF materials [14–15]. Since the early 1990s, electrospinning has been used in preparation of most organic polymer nanofibers [16–17]. Assisted by the development of electrospinning and post-processing methods, the scope of electrospun fibers has been gradually extended from organic nanofibers to inorganic/organic composite nanofibers and inorganic nanofibers. Indeed, a unique type of nanofiber, namely the ACNF, has been prepared by the electrospinning approach and subsequent heat treatment. Because the diameter of nanofibers obtained from electrostatic spinning is within the scale of nanometers to micrometers, and the pore size is

Corresponding author: Yan-bo Wu E-mail: wuyanbo_djd@126.com

within the scale of micrometers, this type of material should exhibit fascinating advantages such as high specific surface area, excellent porosity, light weight, and remarkable mechanical properties. Consequently, it has found applications in the development of filter materials, catalyst support materials, and sensors; moreover, this material can also be employed in the biomedical, electrical, and optical fields [18–20].

Recently, more and more attention has been paid to the study of adsorption capacity of composite fibers prepared by electrostatic spinning methods [21–22]. Several research groups have reported that the adsorption capacity of composite fibers for gas or liquid could be increased by introducing metals or metal oxides into the precursors [23]. The improvement of gas adsorption ability originates from the increase of specific surface area and pore volume, due to the enhancement of precursor pyrolysis promoted by the metal or metal oxide catalysts [24–26]. For instance, Oh *et al.* [27] reported that embedding manganese nanoparticles into the precursor could substantially increase the specific surface area and pore volume, which ultimately would lead to a higher toluene adsorption capacity. On the other hand, Im *et al.* [28] found that vanadium pentoxide embedded in the precursors of ACNF could act as a catalyst for the dissociation of oxygen molecules, and CO or CO_2 molecules were formed during the pyrolysis reaction, leading to an ultra-microporous structure. Indeed, it has been disclosed that the hydrogen adsorption capacity of ACNF could be dramatically improved via this approach, affording an effective hydrogen storage medium.

Although the preparation and application of ACNF composite materials have been widely studied, research on the adsorption performance of the above materials for low concentrations of SO_2 has not been reported, as far as we know. Herein, we report the preparation of three different PAN-based ACNFs via electrostatic spinning, pre-oxidation, and carbonization processes. These materials have been comprehensively characterized by scanning electron microscopy (SEM), thermo-gravimetric-differential scanning calorimetry (TG–DSC), Fourier transform infrared spectroscopy (FT-IR), and X-ray diffraction (XRD) technologies, and their adsorption properties have been studied in detail through low-concentration SO_2 adsorption experiments at room temperature.

2. Experimental

2.1. Starting materials

N,N′-dimethylacetamide (DMAC), cellulose acetate (CA), and silver nitrate (analytical grade) were purchased from China Sinopharm Chemical Reagent Co., Ltd., polyacrylonitrile (PAN) was provided by Sinopec Anqing Petrochemical Company, and the raw materials was dried for 12 h at 40°C before it was ground into a powder material.

2.2. Preparation of precursor solutions

Three precursors (PAN, PAN/CA, and PAN/CA–$AgNO_3$) were dissolved in DMAC to afford 14wt% solutions, in which the mass ratio of PAN to CA was 8:2 and the content of $AgNO_3$ was 5wt%. Subsequently, these precursor solutions were vigorously stirred for 12 h at 40°C in water before they were used for the next step.

2.3. Preparation of fibers by electrostatic spinning

A schematic of the electrospinning setup is shown in Fig. 1. All precursor solutions were loaded into the injector of the electrostatic spinning device. The voltage used for electrostatic spinning was 10 kV and the collection distance was 24 cm. The relative humidity of the room was maintained at 30% ± 10%.

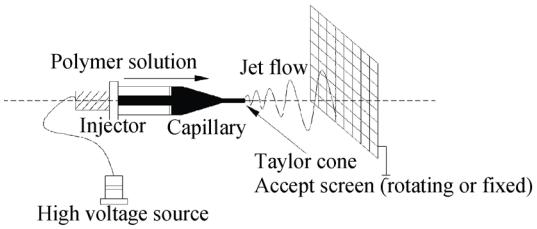

Fig. 1. Schematic diagram of the electrospinning setup.

2.4. Preparation of ACNF

Pre-oxidation of the three PAN-based fibers (PAN, PAN/CA, and PAN/CA–Ag based fibers) was conducted in an air-circulating furnace, in which the temperature was increased from room temperature to 300°C at a rate of 1°C/min, and the fiber material was kept at the final temperature for 90 min. Subsequently, the activated carbon fibers were treated with 1 mol/L H_3PO_4 solution for 1 h, and the reduced materials were carbonized under nitrogen protection. The temperature of carbonization was gradually increased to 800°C at a rate of 5°C/min, followed by holding for 30 min at the final temperature. Finally, ACNFs were washed with deionized water to remove acid residue and dried in a vacuum oven at 110°C.

2.5. Characterization

The viscosity and conductivity of the precursor solutions were measured with a rotational viscometer (Shanghai,

NDJ–1) and a conductivity meter (Shanghai, DDS–11A). Thermo-gravimetric analysis (TG) and differential scanning calorimetry (DSC) (Netzsch STA449 synchronous thermal analyzer) were employed to study the thermostability of ACNFs. The surface appearance of the prepared ACNFs was examined with an SEM (JEOL, ZSM–6360LV). During the course of the pre-oxidation, activation, and carbonization processes, structural changes of the molecular chains and the presence of silver nitrate were monitored by XRD (XRD–6000) and FT-IR (Thermo Finnigan, Nicolet 8700). Finally, the porous structure of ACNFs was investigated by BET analysis (ASAP2020).

2.6. Adsorption of sulfur dioxide under low-concentration conditions

The concentration of SO_2 in the air is usually fairly low, which could be effectively imitated by 0.5vol% SO_2 in N_2. The adsorptive properties of ACNFs were determined according to the national environmental protection standards of People's Republic of China (HJ482—2009). The entire adsorptive apparatus has been assembled in our laboratory, and its schematic diagram is shown in Fig. 2. The flow rate of SO_2 and N_2 was controlled by adjusting the rotor flow meters after opening the globe valves. The target concentration SO_2 diluted by N_2 in the mixing chamber was introduced into the adsorption column. PAN-based fibers adsorbed the low-concentration SO_2 and the tail gas was collected into the absorption bottles containing formaldehyde solution.

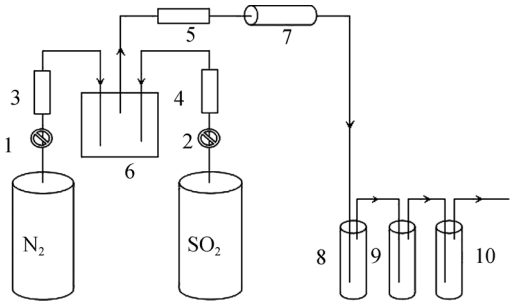

Fig. 2. Schematic diagram of the adsorptive apparatus (1, 2 — Globe valve; 3, 4, 5 — Rotor flow meter; 6 — Mixing chamber; 7 — Adsorption column; 8, 9, 10 — Adsorption bottle).

The adsorption capacity (M) of each fiber material could be calculated from the equation described below:

$$M = \frac{[(0.5\% \times 64 \times Q \cdot T)/22.4 - (m_1 + m_2 + m_3)V \times 10^{-3}]}{M_1},$$

where m is the quantity of sulfur dioxide in the adsorption solution (μg/mL), V is the volume of adsorption solution (mL), Q is the gas flow of 0.5vol% SO_2 in N_2 (mL/min), T is the adsorption time (min), and M_1 is the quantity of ACFs (g). Theoretically, the adsorption performance could be significantly affected by temperature and concentration, which should be extensively varied in order to examine the overall adsorption efficiency.

3. Results and discussion

3.1. Viscosity and conductivity of precursor solutions

The viscosity and conductivity of precursor solutions modified with CA or CA–$AgNO_3$ additives are summarized in Table 1. Specifically, when CA was added into the precursor solution, its viscosity value appeared to be slightly higher, due to the stronger frication force originated from the spiral molecular chains of CA polymer. However, adding CA into the precursor solutions does not substantially affect their conductivity, because CA is a polymer but not an electrolyte. On the other hand, when $AgNO_3$ was added, the conductivity of precursor solutions was significantly improved, because $AgNO_3$ could completely ionize in solutions and ultimately enhanced the conductivity. Generally, adding CA into the precursor solutions could increase the viscosity, whereas adding $AgNO_3$ should improve the conductivity.

Table 1. Viscosity and conductivity of precursor solutions

Precursor solution	Viscosity / (mPa·s)	Conductivity / (mS·cm^{-1})
PAN	839	0.192
PAN/CA	880	0.199
PAN/CA–$AgNO_3$	892	0.546

3.2. TG–DSC analysis

Fig. 3 shows the thermo-gravimetric (TG) curves of the three fiber materials. In Fig. 3(a), a four-stage process was observed during the course of degradation. Initially, no weight loss was evident in the TG curve before 280°C. However, because the intramolecular cyclization reaction and dehydrogenation reaction often take place within the range of 280 to 350°C, a heat-resistant trapezoidal structure should be produced accompanied by the release of pyrolytic gases, which ultimately would lead to the most obvious weight-loss peak in the overall spectra. Indeed, the DSC curves showed an obvious peak at 315°C, and a 30wt% weight loss was observed, indicating violent reactions and maximal weight-loss rate. Within the range of 350 to 500°C, fibers with a trapezoidal structure could undergo crosslinking and condensation reactions to generate turbostratic ma-

terials. Simultaneously, the oxygen-containing functionalities could be eliminated as small oxygen-containing molecules, affording a slow weight loss (20wt%). After the temperature reached 500°C, a full turbostratic structure was obtained and all of the oxygen-containing groups were removed, eventually leading to a stable fiber structure.

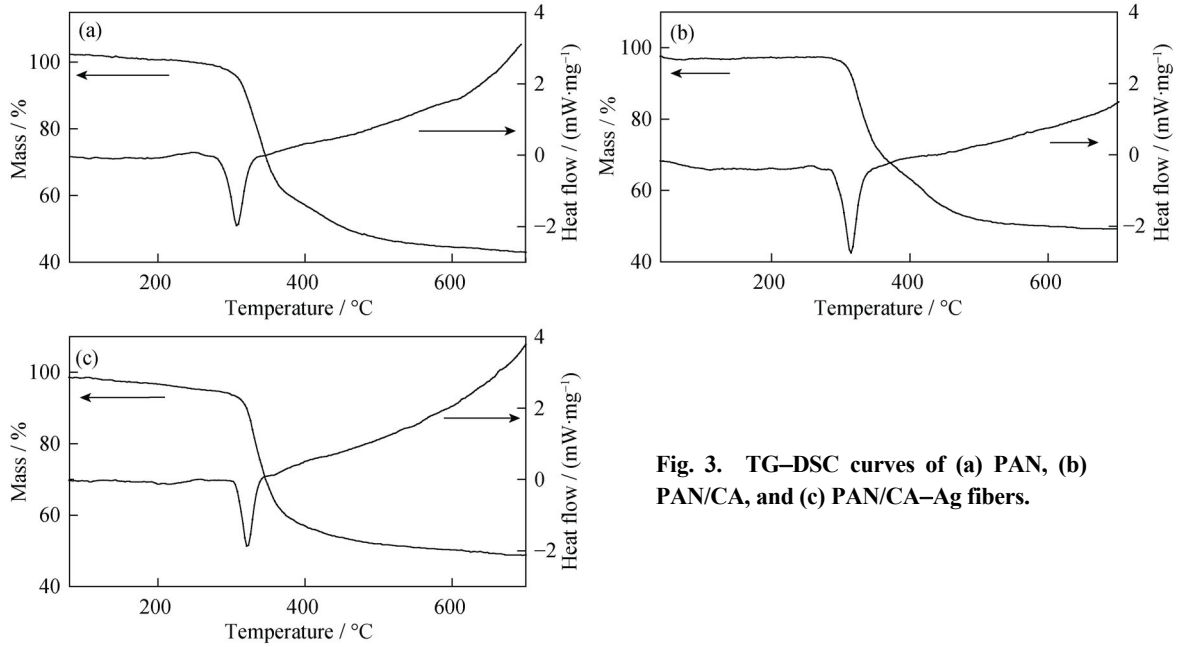

Fig. 3. TG–DSC curves of (a) PAN, (b) PAN/CA, and (c) PAN/CA–Ag fibers.

The weight-loss stages, overall DSC curves, and peak temperatures shown in Figs. 3(b) and 3(c) are similar to the ones in Fig. 3(a), which indicates that the addition of CA or Ag did not significantly impact the thermal decomposition process of PAN materials. However, it was found that the total weight loss in Fig. 3(b) (52wt%) and Fig. 3(c) (52wt%) was less than the one in Fig. 3(a) (57wt%), demonstrating that the yields of fibers could be substantially improved by introduction of CA or Ag.

3.3. SEM analysis

SEM images of the produced PAN, PAN/CA, and PAN/CA–Ag fibers are shown in Fig. 4. The morphological characters demonstrated in Figs. 4(a_1), 4(b_1), and 4(c_1) clearly indicate that PAN fibers possessed remarkable spinning ability and the diameters of the original fibers were 730, 508, and 326 nm, respectively. Furthermore, fibers shown in Figs. 4(b_1) and 4(c_1) appear to be bifurcated, which adequately suggests that PAN and CA were not compatible materials and became immiscible during the spinning process, even though they were completely dissolved in DMAC. As shown in Fig. 4(c_1), the addition of $AgNO_3$ could significantly improve the conductivity of the precursor solution, but the diameter of the fibers became uneven, because the solution was overwhelmingly stretched in the electric field.

The surface of pre-oxidized original fibers became collapsible and adhesive, and their diameters were substantially increased, as illustrated in Figs. 4(a_2), 4(b_2), and 4(c_2). These results indicate that solvent residues in the fibers were completely removed via evaporation. As demonstrated in Figs. 4(a_3), 4(b_3), and 4(c_3), after the carbonization process, the fibers became thinner and carbon in the materials was enriched, due to the elimination of hydrogen, oxygen, and nitrogen.

3.4. FT-IR analysis

Fig. 5 shows the FT-IR spectra of original PAN-based fibers, pre-oxidized fibers, and fibers prepared after activation and carbonization. As illustrated in Fig. 5(a), the band at 2249 cm^{-1} should be attributed to the stretching vibration of C≡N bonds, which is the characteristic band of PAN materials, suggesting that adding CA or $AgNO_3$ would not alter the molecular structure of fibers. However, the characteristic band of pre-oxidized PAN fibers shifted to 2233 cm^{-1} and its vibration intensity was greatly diminished, as shown in Fig. 5(b). At the same time, the stretching vibration of the C=C bond at 1597 cm^{-1} appeared to be stronger, which indicated that most of the C≡N bonds were demolished and a large number of C=C bonds were formed after the pre-oxidation treatment at 300°C. Interestingly, Fig. 5(c) demonstrates that the band of C≡N stretching vibration was

at 1585 cm^{-1} for PAN fibers and PAN/CA fibers; however, PAN/CA–Ag fibers exhibited a band at 1630 cm^{-1}, corresponding to the stretching vibration of C=C bonds of the fiber material, which was carbonized at 800°C under nitrogen protection. Based on the results obtained from IR spectral analysis, we concluded that the molecular structures of PAN or CA, which were originally composed of C≡N, C–O, and C=O bonds, had been completely converted to carbon structures incorporated with C=C bonds during the process of pre-oxidation, activation, and carbonization.

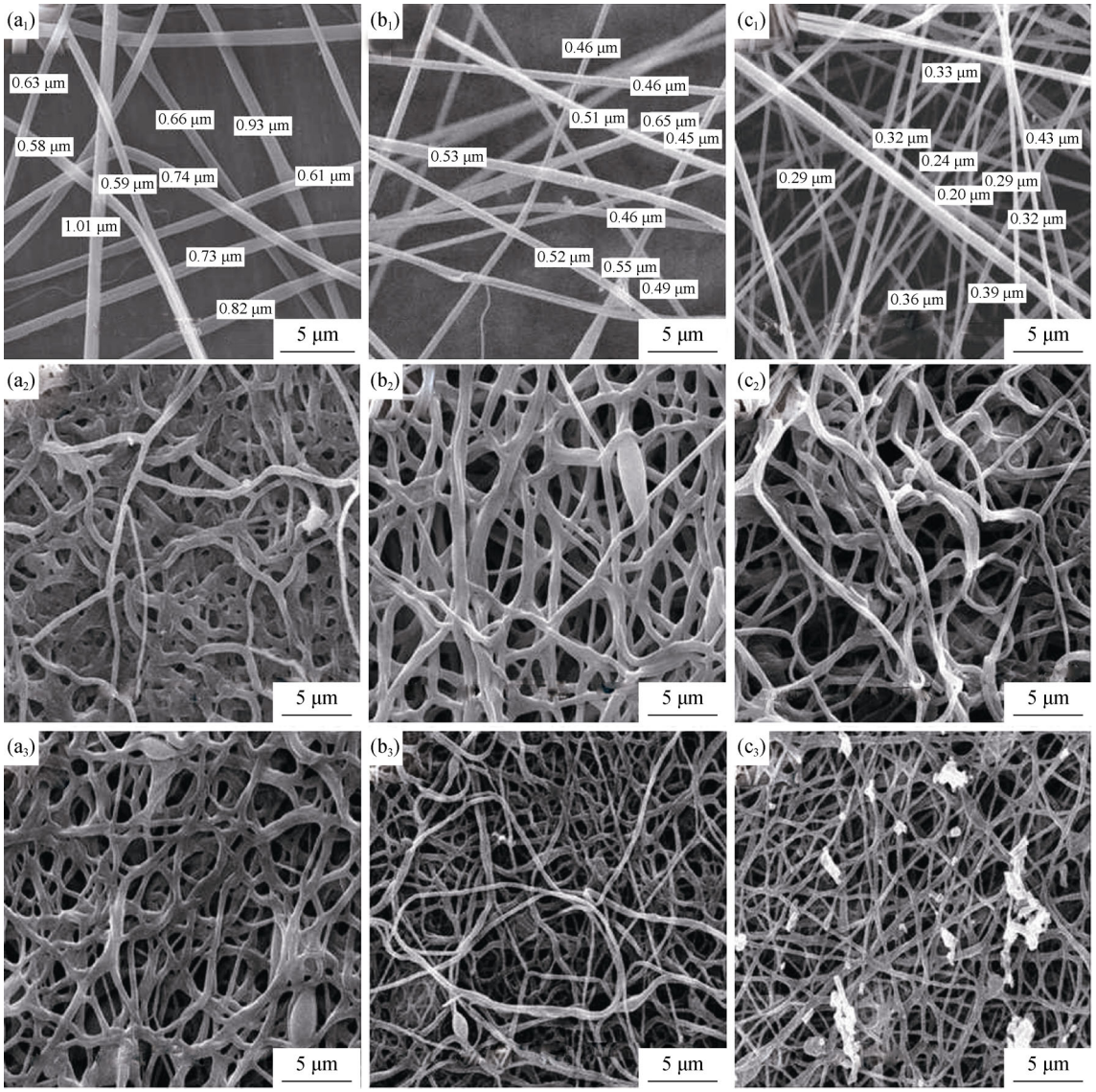

Fig. 4. SEM images of fibers: the top row shows original fibers; the middle and bottom rows show fibers after pre-oxidation and fibers after carbonization and activation, respectively.

3.5. XRD analysis

The XRD spectra of PAN, PAN/CA, and PAN/CA–Ag based ACNFs are illustrated in Fig. 6. Specifically, all XRD spectra exhibited a diffraction peak at 24°, which typically corresponds to a turbostratic structure, suggesting that this type of structure was present in all ACNFs. The strong diffraction peaks at 2θ = 37.99°, 44.15°, 64.22°, 77.11°, and 81.23° in curve *c* are the characteristic peaks of element Ag (JCPDS card No. 03–065–8452), which means that Ag was doped in the PAN/CA–Ag based ACNF by decomposition of $AgNO_3$ at high temperature.

3.6. BET analysis

The BET results of PAN, PAN/CA, and PAN/CA–Ag based ACNFs in Table 2 show that the fibers' surface area and micropore volume increased because of the incorporation of CA and Ag, contributing to the improvement of their ability to adsorb gas. Particularly, PAN/CA–Ag based

ACNF exhibited the best porosity features, such as largest specific surface area (1176.5 m^2/g) and excellent pore content, indicating that this material may be considered as the most promising candidate for gas adsorption.

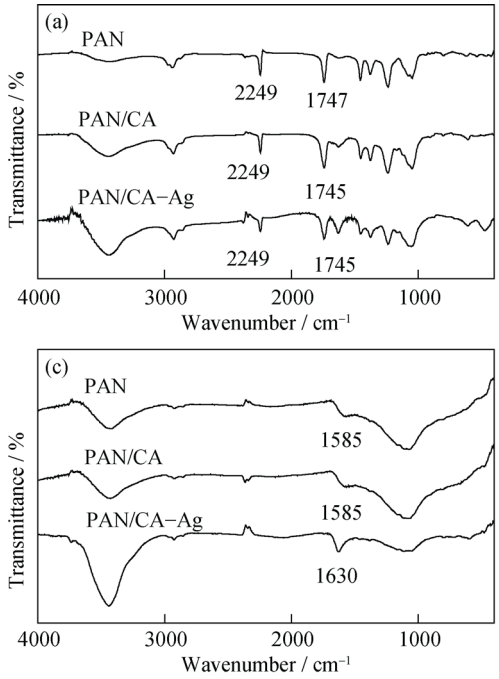

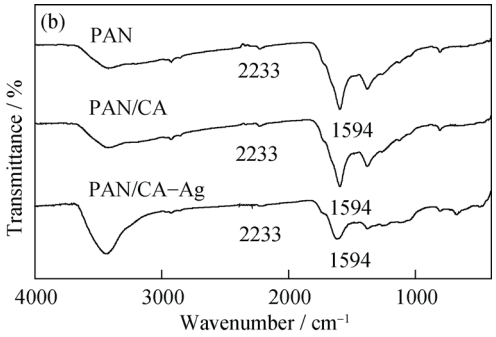

Fig. 5. FT-IR spectra of (a) original fibers, (b) fibers after pre-oxidation, and (c) fibers after carbonization and activation.

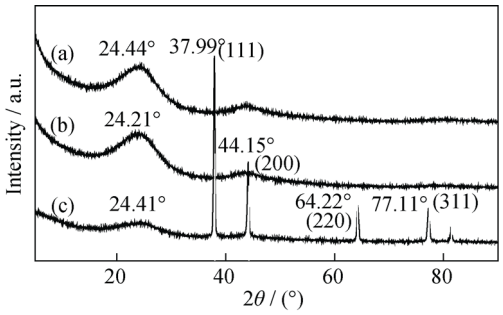

Fig. 6. XRD spectra of PAN-based ACNFs: (a) PAN, (b) PAN/CA, and (c) PAN/CA−Ag.

Table 2. Pore volume and specific surface area of original PAN, PAN/CA, and PAN/CA−Ag based ACNFs

Sample	Specific surface area / ($m^2 \cdot g^{-1}$)	Total pore volume / ($cm^3 \cdot g^{-1}$)	Micropore volume / ($cm^3 \cdot g^{-1}$)	Mesopore volume / ($cm^3 \cdot g^{-1}$)
PAN	984	0.3927	0.3496	0.0431
PAN/CA	1038.5	0.5087	0.4833	0.0254
PAN/CA−Ag	1176.5	0.5913	0.5617	0.0296

3.7. Adsorption of PAN-based ACNFs on low concentrations of SO_2

The adsorption effects of these fibers at different temperatures are summarized in Fig. 7. The total flow rate was 1000 mL/min and the SO_2 concentration was 1 μg/mL, and the amount of PAN-based ACNF in the adsorption column was 1 g. Notably, their adsorption capacity appears to be decreased at higher temperatures, which is consistent with the typical characters of physical adsorption. Because higher temperatures can promote the thermal motion of gas molecules, their residing time on the fiber surface should be reduced, which would enable them to rapidly desorb the adsorbed SO_2 molecules and ultimately alter the adsorption outcome. On the contrary, lower temperatures generally favor the adsorption process. The PAN/CA−Ag based ACNF prepared in our laboratory exhibited the most promising adsorption effect. However, all three adsorption capacity curves started to converge when the adsorption temperature reached 80°C.

Fig. 8 shows the effect of SO_2 concentration on the adsorption performance of different ACNFs. The total flow rate was 1000 mL/min and the adsorption temperature was 20°C, and the amount of PAN-based ACNF in the adsorption column was 1 g. Interestingly, the adsorption efficiency of the fibers was dramatically reduced when a higher concentration of SO_2 was employed, indicating a potential long-term application under lower-concentration conditions. Indeed, SO_2 molecules usually face less completion from other molecules under lower-concentration conditions, resulting in a decrease of the adsorption capacity. In the presence of a high concentration of SO_2, the fibers' adsorption

capacity could rapidly reach saturation and a large concentration gradient between fibers and the adsorption gas would be generated, which should substantially increase the diffusion momentum of gas molecules, enabling SO_2 to pass through the fiber surface at a faster rate. Furthermore, SO_2 molecules could also penetrate into the fiber interior, thus its saturation adsorption capacity curve should exhibit a slight increase. The adsorption efficiency of PAN/CA–Ag based ACNF under different SO_2 concentration conditions appears to be superior, because it possesses a fascinating porosity property originated from the thermal decomposition of $AgNO_3$. In addition, its specific surface area and pore volume are both higher than those of other two fibers, indicating that this material should contribute more to SO_2 adsorption.

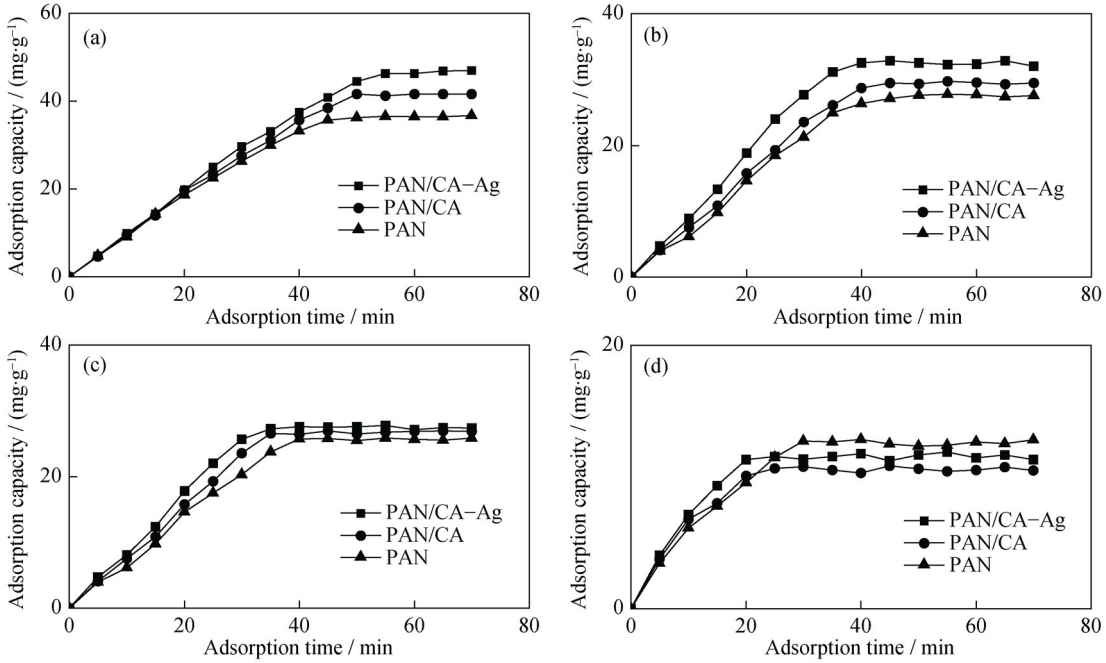

Fig. 7. Adsorption capacity of ACNFs for SO_2 at different temperatures: (a) 20°C; (b) 40°C; (c) 60°C; (d) 80°C.

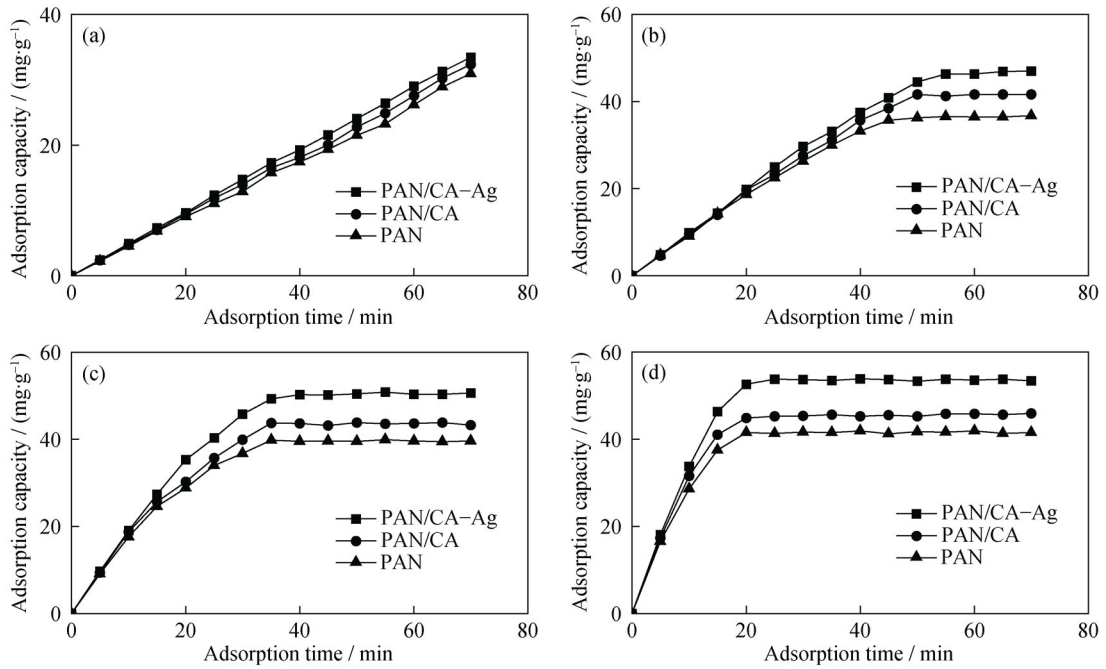

Fig. 8. Adsorption capacity of ACNFs for SO_2 at different concentrations: (a) 0.5 μg/mL; (b) 1.0 μg/mL; (c) 2.0 μg/mL; (d) 4.0 μg/mL.

4. Conclusions

(1) Three PAN-based ACNFs were successfully prepared by an electrospinning method. The morphological study during the course of preparation, pre-oxidation, carbonization, and activation was deliberately conducted by means of viscosity, conductivity, and SEM technologies. The weight-loss stages and DSC curves of these fibers were very similar, which indicated that the addition of CA or Ag did not significantly impact the thermal decomposition of PAN materials but the yield of the fibers increased to some extent.

(2) FT-IR analysis indicated that the linear structure of PAN and CA molecules fractured, while the cyclized and trapezoidal structure formed during the treatment stage. After carbonization and activation processes, the molecular structure composed of C≡N and C–O bonds was mostly converted to a carbon scaffold incorporated with C=C bonds. A diffraction peak at 24° in XRD spectra typically corresponded with a turbostratic structure and the strong characteristic diffraction peaks were evidence that silver existed in the PAN/CA–Ag based ACNF. BET analysis showed that the fibers' surface area and micropore volume were increased by the incorporation of CA and Ag. Particularly, PAN/CA–Ag based ACNF material exhibited the best porosity feature.

(3) SO_2 adsorption experiments indicated that all the three fiber materials exhibited good adsorption effects for lower concentrations of SO_2 at room temperature; especially, the PAN/CA–Ag based ACNF showed the best adsorption performance, and it may be one of the most promising adsorbents.

Acknowledgements

This work was financially supported by the Natural Science Foundation of China (Nos. 21076028 and 50802010).

References

[1] G. Wang, C. Pan, L.P. Wang, Q. Dong, C. Yu, Z.B. Zhao, and J.S. Qiu, Activated carbon nanofiber webs made by electrospinning for capacitive deionization, *Electrochim. Acta*, 69(2012), p. 65.

[2] R. Yang, J.H. Liu, and S.M. Li, Preparation and characterization of in-site regenerated TiO_2–ACFs photocatalyst, *Int. J. Miner. Metall. Mater.*, 18(2011), No. 3, p. 357.

[3] M.A. Sidheswaran, H. Destaillats, D.P. Sullivan, S. Cohn, and W.J. Fisk, Energy efficient indoor VOC air cleaning with activated carbon fiber (ACF) filters, *Build. Environ.*, 47(2012), p. 357.

[4] S. Adapa, V. Gaur, and N. Verma, Catalytic oxidation of NO by activated carbon fiber (ACF), *Chem. Eng. J.*, 116(2006), No. 1, p. 25.

[5] V. Gaur, A. Sharma, and N. Verma, Preparation and characterization of ACF for the adsorption of BTX and SO_2, *Chem. Eng. Process.*, 45(2006), No. 1, p. 1.

[6] V. Gaur, R. Asthana, and N. Verma, Removal of SO_2 by activated carbon fibers in the presence of O_2 and H_2O, *Carbon*, 44(2006), No. 1, p. 46.

[7] V. Gaur, A. Sharma, and N. Verma, Catalytic oxidation of toluene and *m*-xylene by activated carbon fiber impregnated with transition metals, *Carbon*, 43(2005), No. 15, p. 3041.

[8] V. Gaur, A. Sharma, and N. Verma, Removal of SO_2 by activated carbon fibre impregnated with transition metals, *Can. J. Chem. Eng.*, 85(2007), No. 2, p. 188.

[9] J.Y. Wang, F.Y. Zhao, Y.Q. Hu, R.H. Zhao, and R.J. Liu, Modification of activated carbon fiber by loading metals and their performance on SO_2 removal, *Chin. J. Chem. Eng.*, 14(2006), No. 4, p. 478.

[10] P. Lu, C.T. Li, G.M. Zeng, L.J. He, D.L. Peng, H.F. Cui, S.H. Li, and Y.B. Zhai, Low temperature selective catalytic reduction of NO by activated carbon fiber loading lanthanum oxide and ceria, *Appl. Catal. B*, 96(2010), No. 1-2, p. 157.

[11] R.S. Rathore, D.K. Srivastava, A.K. Agarwal, and N. Verma, Development of surface functionalized activated carbon fiber for control of NO and particulate matter, *J. Hazard. Mater.*, 173(2010), No. 1-3, p. 211.

[12] D. Esrafilzadeh, M. Morshed, and H. Tavanai, An investigation on the stabilization of special polyacrylonitrile nanofibers as carbon or activated carbon nanofiber precursor, *Synth. Met.*, 159(2009), No. 3-4, p. 267.

[13] J. Zhu, A. Holmen, and D. Chen, Carbon nanomaterials in catalysis: proton affinity, chemical and electronic properties, and their catalytic consequences, *ChemCatChem*, 5(2013), No. 2, p. 378.

[14] R.M. Singhal, A. Sharma, and N. Verma, Micro-nano hierarchal web of activated carbon fibers for catalytic gas adsorption and reaction, *Ind. Eng. Chem. Res.*, 47(2008), No. 10, p. 3700.

[15] A.K. Gupta, D. Deva, A. Sharma, and N. Verma, Adsorptive removal of fluoride by micro-nanohierarchal web of activated carbon fibers, *Ind. Eng. Chem. Res.*, 48(2009), No. 21, p. 9697.

[16] W.E. Teo, R. Inai, and S. Ramakrishna, Technological advances in electrospinning of nanofibers, *Sci. Technol. Adv. Mater.*, 12(2011), No. 1, p. 1.

[17] T. Subbiah, G.S. Bhat, R.W. Tock, S. Parameswaran, and S.S. Ramkumar, Electrospinning of nanofibers, *J. Appl. Polym. Sci.*, 96(2005), No. 2, p. 557.

[18] W.K. Son, J.H. Youk, T.S. Lee, and W.H. Park, The effects of solution properties and polyelectrolyte on electrospinning of ultrafine poly (ethylene oxide) fibers, *Polymer*, 45(2004), No. 9, p. 2959.

[19] H.W. Song, H.Q. Yu, G.H. Pan, X. Bai, B. Dong, X.T. Zhang,

and S.K. Hark, Electrospinning preparation, structure, and photoluminescence properties of $YBO_3:Eu^{3+}$ nanotubes and nanowires, *Chem. Mater.*, 20(2008), No. 14, p. 4762.

[20] K.S. Yang, Y.J. Yoon, M.S. Lee, W.J. Lee, and J.H. Kim, Further carbonization of anisotropic and isotropic pitch-based carbons by microwave irradiation, *Carbon*, 40(2002), No. 6, p. 897.

[21] H.Q. Yu, Y.B. Wu, T.B. Song, Y. Li, and Y. Shen, Preparation of metal oxide doped ACNFs and their adsorption performance for low concentration SO_2, *Int. J. Miner. Metall. Mater.*, 20(2013), No. 11, p. 1102.

[22] B. Cagnon, X. Py, A. Guillot, and F. Stoeckli, The effect of the carbonization/activation procedure on the microporous texture of the subsequent chars and active carbons, *Microporous Mesoporous Mater.*, 57(2003), No. 3, p. 273.

[23] J.S. Im, S.J. Park, T. Kim, and Y.S. Lee, Hydrogen storage evaluation based on investigations of the catalytic properties of metal/metal oxides in electrospun carbon fibers, *Int. J. Hydrogen Energy*, 34(2009), No. 8, p. 3382.

[24] S.K. Nataraj, B.H. Kim, J.H. Yun, D.H. Lee, T.M. Aminabhavi, and K.S. Yang, Effect of added nickel nitrate on the physical, thermal and morphological characteristics of polyacrylonitrile-based carbon nanofibers, *Mater. Sci. Eng B*, 162(2009), No. 2, p. 75.

[25] J.M. Oh, A.S. Kumbhar, O. Geiculescu, and S.E. Creager, Mesoporous carbon/zirconia composites: a potential route to chemically functionalized electrically-conductive mesoporous materials, *Langmuir*, 28(2012), No. 6, p. 3259.

[26] C. Tekmen, Y. Tsunekawa, and H. Nakanishi, Electrospinning of carbon nanofiber supported Fe/Co/Ni ternary alloy nanoparticles, *J. Mater. Process. Technol.*, 210(2010), No. 3, p. 451.

[27] G.Y. Oh, Y.W. Ju, H.R. Jung, and W.J. Lee, Preparation of the novel manganese-embedded PAN-based activated carbon nanofibers by electrospinning and their toluene adsorption, *J. Anal. Appl. Pyrolysis*, 81(2008), No. 2, p. 211.

[28] J.S. Im, O. Kwon, Y.H. Kim, S.J. Park, and Y.S. Lee, The effect of embedded vanadium catalyst on activated electrospun CFs for hydrogen storage, *Microporous Mesoporous Mater.*, 115(2008), No. 3, p. 514.